Dynamics of scroll rings in a parameter gradient

Michael Vinson*
Department of Physics, Shippensburg University, Shippensburg, Pennsylvania 17257

Arkady Pertsov
Department of Pharmacology, SUNY Health Science Center, Syracuse, New York 13210
(Received 12 August 1998)

Experimental observations of scroll rings in excitable media have shown that an externally applied parameter gradient can significantly alter the dynamics of the ring, leading to rotation of the plane of the ring, variations in its rate of collapse, and distortions in its shape. Here we propose a theory to account for these effects by extending the theory of local filament dynamics to include the influence of the parameter gradient. Numerical simulations using the FitzHugh-Nagumo equations show that the proposed theory works well when the differences in rotation periods at different parts of the filament are sufficiently small. When this condition does not hold, the theory must be modified to take into account nonlocal interactions.
[S1063-651X(99)10403-3]

PACS number(s): 82.40.Ck, 82.20.Wt

I. INTRODUCTION

Excitable media describe systems ranging from the biological to the chemical [1–5]. These systems often exhibit periodic excitations in the form of spiral waves. In three dimensions these waves are called scroll waves, and they rotate about a one-dimensional singularity, the filament. In the simplest case the filament is a straight line, but it may also be curved; when it forms a circle, the resulting wave pattern is known as a scroll ring. See Fig. 1. Most studies to date have concentrated on the dynamics of these waves in homogeneous media. In natural systems, however, such as the Belousov-Zhabotinsky (BZ) chemical reaction and cardiac tissue, the waves usually propagate in the presence of inhomogeneities [6,7,1,8–10]. In this paper, we concentrate on the behavior of scroll rings in the presence of a large-scale inhomogeneity. The simplest model of such an inhomogeneity is a smooth parameter gradient, which can dramatically affect the dynamics of scroll waves [11,9,7,12–15].

A scroll ring in a homogeneous excitable medium generally shrinks until it self-annihilates, and it may also drift along its axis of symmetry; however, its axis of symmetry remains fixed in space and the ring itself remains circular [16,17]. Recent experimental observations of scroll rings in a BZ reaction with a temperature gradient [14] revealed that the addition of a parameter gradient can lead to reorientation of the axis of the ring, change the rate at which it shrinks (and in some cases even reverse the shrinking), and may in addition alter the circular shape of the ring. It is the goal of the present paper to account for these effects with a quantitative, predictive theory.

We do this by considering the extension of the theory of local filament dynamics [18–21] to include an inhomogeneous medium with a smooth parameter gradient. In two dimensions, such a gradient induces a drift velocity of the center of rotation [9,22,12]. In three dimensions a similar drift occurs, though it may have more complicated effects on the filament motion [12,10,13]. Earlier investigations [12–14] have shown that gradient-induced drift can be combined with the local theory to give qualitative agreement with simulations [12] and experiment [13,14]. In the present paper, we further develop this approach, obtaining a quantita-

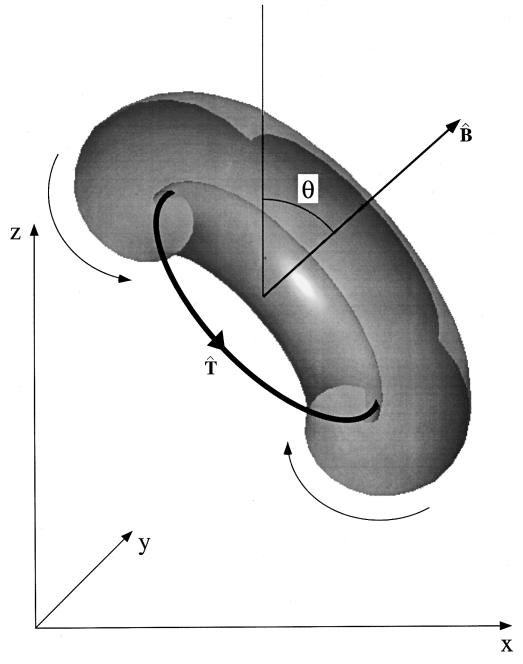

FIG. 1. Schematic of a scroll ring. The ring is shown in cross section. The filament about which the wave rotates is shown as a heavy black curve. The unit vector $\hat{\mathbf{T}}$ is tangent to the filament. The binormal unit vector $\hat{\mathbf{B}}$ lies along the axis of symmetry of the ring, and is inclined by an angle θ (rotated about the y axis) with respect to the z direction.

*Author to whom correspondence should be addressed. Present address: Department of Physics, American University of Sharjah, P.O. Box 26666, Sharjah, U.A.E. Electronic address: mjv@cutter.ship.edu

tive theory for the motion of a scroll ring in a medium with a gradient. We also obtain analytic estimates of the range of applicability of the theory, based on the influence of nonlocal self-interactions of the scroll ring filament. We test the predictions of the theory numerically using the FitzHugh-Nagumo equations [23,24,10].

II. EQUATIONS OF MOTION IN A PARAMETER GRADIENT

In this section we extend the equations of local filament dynamics to include the influence of a parameter gradient. We focus here only on the equations that describe the evolution of the shape of the vortex ring filament, without attempting to model the development of twist. The theory of local filament dynamics [18–21], derived under the assumption of a homogeneous medium, gives approximate equations for the velocity $d\mathbf{R}(p)/dt$ of each point p of the filament in terms of the local curvature κ and (in principle) torsion τ and twist rate w. In an inhomogeneous medium, we assume that weak, smooth inhomogeneities may be accounted for by adding the gradient-induced drift velocity to the local filament equations [12–14]. Using only the leading-order filament dynamics equations given in [21,20], we therefore postulate that

$$\frac{d\mathbf{R}(p)}{dt} = \alpha\kappa(p)\hat{\mathbf{N}}_p + \mu\kappa(p)\hat{\mathbf{B}}_p + \mathbf{G}_p, \tag{1}$$

where $\hat{\mathbf{N}}_p$ is the local unit vector normal to the curve of the filament at location p, $\hat{\mathbf{B}}_p$ is the local binormal unit vector, $\mathbf{G}_p$ is the gradient-induced velocity at p, and α and μ (called, respectively, b_2 and c_3 in [20,21]) are constants that depend on the parameters of the medium. For a scroll ring, α (sometimes refered to as the filament tension [21]) describes the shrinking of the ring, and μ describes its motion along its axis of symmetry (binormal drift). (Note that $\mu=0$ for equal-diffusion systems such as the BZ model [25,26]). In writing Eq. (1), we make use of the fact that to leading order, the motion of the filament is independent of its twist and torsion [21]. The presence of the gradient will certainly lead to twist, but provided it remains sufficiently small, Eq. (1) should still hold.

The term $\mathbf{G}_p$ in Eq. (1) accounts for the effect of the gradient on the local filament velocity. Numerical [22,12] and experimental [13,14] observations of drifting spiral waves indicate that for a gradient oriented in the $\hat{\mathbf{z}}$ direction, the resulting drift velocity may be written

$$\begin{aligned}\mathbf{G} &= \beta(g)\hat{\mathbf{T}}\times\hat{\mathbf{z}} + \gamma(g)\hat{\mathbf{z}} \\ &\equiv \mathbf{G}_\perp + \mathbf{G}_\parallel,\end{aligned} \tag{2}$$

where $\hat{\mathbf{T}}$ is a unit vector tangential to the filament, and $\beta(g)$ and $\gamma(g)$ are functions of the gradient strength g and describe, respectively, the components of the drift velocity perpendicular to and parallel to the gradient direction. We emphasize that these functions may be determined from *two-dimensional* observations (see final paragraph of this section).

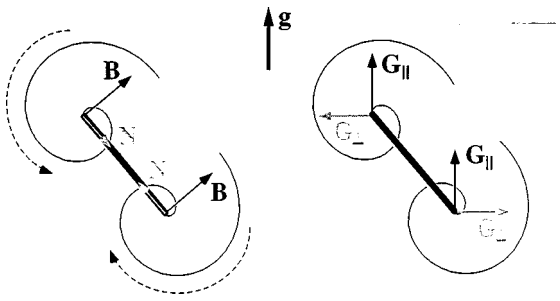

FIG. 2. Schematic diagram of the velocities induced on a scroll ring by (a) local filament dynamics, and (b) the gradient. **N** and **B** are, respectively, the normal and binormal velocities. The two components of the gradient-induced drift velocity are $\mathbf{G}_\perp$ and $\mathbf{G}_\parallel$. The gradient is depicted as the vector **g**.

So far our discussion has been quite general. We now specialize to the case of a planar, circular scroll ring. Figure 2 shows schematically the lateral projection of such a ring, with the filament depicted as a black line, along with the vectors **N** and **B** (left panel), and $\mathbf{G}_\perp$ and $\mathbf{G}_\parallel$ (right panel). The normal velocity **N** is oriented inward, causing the ring to shrink. The binormal velocity **B** causes translation of the ring along its axis of symmetry. The gradient-induced velocities also affect the motion of the ring. The parallel component $\mathbf{G}_\parallel$ translates the ring in the direction of the gradient (vertical direction in Fig. 2). The perpendicular component $\mathbf{G}_\perp$ always points in opposite directions at opposite points in the scroll ring (due to the chirality dependence of the perpendicular component of the drift velocity), causing a net ''torque'' (when $\theta\neq 0,\ \pi$) that tends to reorient the plane of the ring.

We now apply Eqs. (1) and (2) to a scroll ring. We therefore consider a ring of radius r, inclined by an angle θ with respect to the direction of the gradient (taken to be the z direction), with center at $\mathbf{a}_c=(x,0,z)$, parametrized as

$$\begin{aligned}\mathbf{R}(p) &= \mathbf{a}_c + \mathbf{r}(p) \\ &= x\hat{\mathbf{x}} + z\hat{\mathbf{z}} + r\cos p\,\hat{\mathbf{y}} - r(\cos\theta\hat{\mathbf{x}} + \sin\theta\hat{\mathbf{z}})\sin p.\end{aligned} \tag{3}$$

Here p parametrizes the curve and runs from 0 to 2π, starting at the point (x,r,z). In writing this parametrization, we assume that when a gradient is added, the ring remains planar and circular (as it does in a homogeneous medium). Appendix C addresses the question of whether the solutions we obtain from this parametrization are stable solutions of the full equations of motion, Eq. (1).

By applying this parametrization to the right-hand side of Eq. (1), and using the fact that for a circular ring, κ is just $1/r$ everywhere, we obtain (see Appendix A for details)

$$\begin{aligned}\frac{d\mathbf{R}(p)}{dt} = &-\frac{\alpha}{r}\cos p\,\hat{\mathbf{y}} + \frac{\alpha}{r}\sin p(\cos\theta\hat{\mathbf{x}} + \sin\theta\hat{\mathbf{z}}) \\ &-\frac{\mu}{r}(\sin\theta\hat{\mathbf{x}} - \cos\theta\hat{\mathbf{z}}) \\ &-\beta(g)(\sin p\,\hat{\mathbf{x}} + \cos\theta\cos p\,\hat{\mathbf{y}}) + \gamma(g)\hat{\mathbf{z}}.\end{aligned} \tag{4}$$

Using Eq. (3) to evaluate the left-hand side of Eq. (4) and equating components, we are left with equations for $r(t)$, $\theta(t)$, $x(t)$, and $z(t)$:

$$
\begin{aligned}
dr/dt &= -\frac{\alpha}{r} + \beta(g)\cos\theta, \\
d\theta/dt &= -\frac{\beta(g)}{r}\sin\theta, \\
dx/dt &= -\frac{\mu}{r}\sin\theta, \\
dz/dt &= \frac{\mu}{r}\cos\theta + \gamma(g).
\end{aligned}
\tag{5}
$$

The first of Eqs. (5) describes the combined effect of the local-dynamics normal velocity (the $-\alpha/r$ term) and the perpendicular component of the drift velocity ($\mathbf{G}_\perp$). The second of Eqs. (5) describes the ''torque'' on the ring due to $\mathbf{G}_\perp$. The third and fourth equations describe the translation of the ring due to the binormal velocity (the μ terms) and $\mathbf{G}_\parallel$. These last two equations do not affect the ring's radius, orientation, or shape.

Analysis of Eqs. (5) leads to the following conclusions. First, the gradient-induced drift affects the contraction of the ring, and may even reverse it. As can be seen from the first of Eqs. (5), when $|\theta| > \pi/2$, the gradient-induced drift accelerates the shrinking of the ring (we choose the z axis such that β is positive). For other angles, the drift opposes the shrinking. When the gradient is sufficiently strong and the ring sufficiently large, the $\beta(g)\cos\theta$ term dominates the $-\alpha/r$ term, and causes the ring to expand. Second, as can be seen from the equation for $d\theta/dt$, the gradient produces a ''torque,'' which reduces $|\theta|$ toward zero. Third, the drift of the ring in the presence of a gradient is no longer along its axis of symmetry, but in addition it acquires a component in the direction of the gradient. The tendency toward expansion and rotation is reminiscent of a current loop in an external magnetic field.

Figure 3 shows the solutions of the first two equations as depicted in (r,θ) phase space. The equations have a hyperbolic fixed point at $(r,\theta)=(\alpha/\beta,0)$. The unstable manifold of this fixed point is the $\theta=0$ axis, and the stable manifold, which forms a separatrix between rings which will shrink to zero radius and rings which will grow indefinitely, is depicted as a dashed curve in Fig. 3. It should be noted that our equations predict growth of a scroll ring even though the filament tension [21,27] is positive, when the gradient is sufficiently strong. This gradient-induced growth of a scroll ring has been observed experimentally in the BZ reaction, in which rings normally collapse [14].

To test our theory quantitatively, we used numerical simulations of a reaction-diffusion equation with FitzHugh-Nagumo kinetics (see Appendix B). To obtain numerical values of the parameters of Eqs. (5), we did the following: α and μ were determined by measuring, respectively, the shrink rate and binormal drift velocity of scroll rings in a *homogeneous* medium; β and γ were determined by measuring the components of the drift velocity of spiral waves in a *two-dimensional* medium with a gradient. The solutions of Eqs. (5), which now have no adjustable parameters, were then compared to the results of the three-dimensional simulations in a medium with a gradient. In the simulations, we

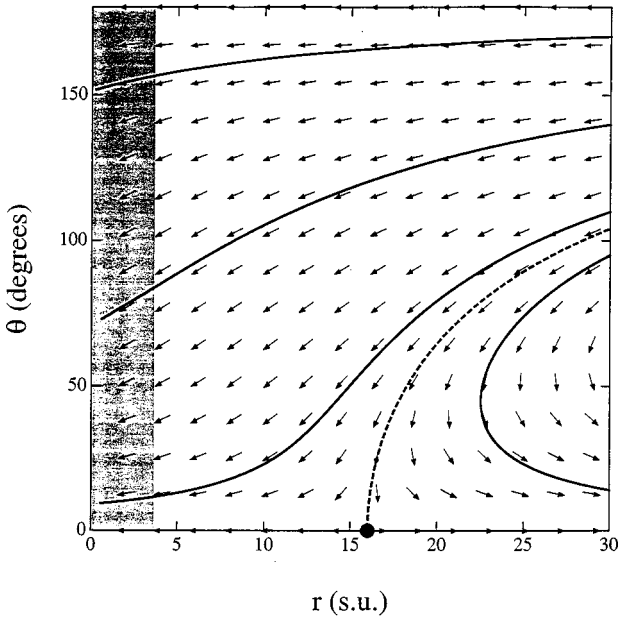

FIG. 3. Phase plane (r,θ) of Eqs. (5). r is shown in space units (s.u.). Here $\alpha=0.24$ and $\beta=0.015$. The arrows are all normalized to the same length. The solid lines are four representative solutions, and the gray band shows the radius below which the ring disappears. The dashed line is the stable manifold of the fixed point (black dot) at $(r,\theta)=(\alpha/\beta,0)$; this manifold separates solutions that will shrink from solutions that will grow indefinitely.

initiated a scroll ring, and applied the gradient after one full turn of the scroll (defining $t=0$ as the moment the gradient was applied). We determined the filament by Fourier smoothing of the core (see Appendix B). The simulations show that the modified local theory gives quantitatively accurate results when the initial angle is small, for a broad range of gradient strength and initial radius (see below). Figure 4 shows a comparison of Eqs. (5) with results from such a simulation, for a case in which the initial angle, θ_0, was 9.8°. The three panels show the time dependence of r, θ, and z for simulations with positive, zero, and negative gradients. As can be seen from Fig. 4(a), the positive gradient (filled triangles) slows down the contraction of the ring relative to the zero-gradient case (circles and dashed line). The negative gradient (open triangles) accelerates the contraction. In all three cases, good agreement between theory (lines) and simulation (symbols) can be seen. The evolution of the z position of the ring and the angle θ also agree with the modified local theory [Figs. 4(b) and 4(c)].

III. NONLOCAL EFFECTS

When the initial angle of the ring is increased, there appear increasing deviations between the predictions of the local theory and the numerical and experimental [14] observations. Figure 5 shows an example of the quantitative deviations from the local theory, for a scroll ring with an initial angle of $\theta_0=46°$. The simulations agree with the theory for some time, but then, after a certain delay, characterized by T_{uw} (see below), they begin to deviate.

In [28], Winfree listed a variety of conditions under which the local theory may fail. In the case under consideration

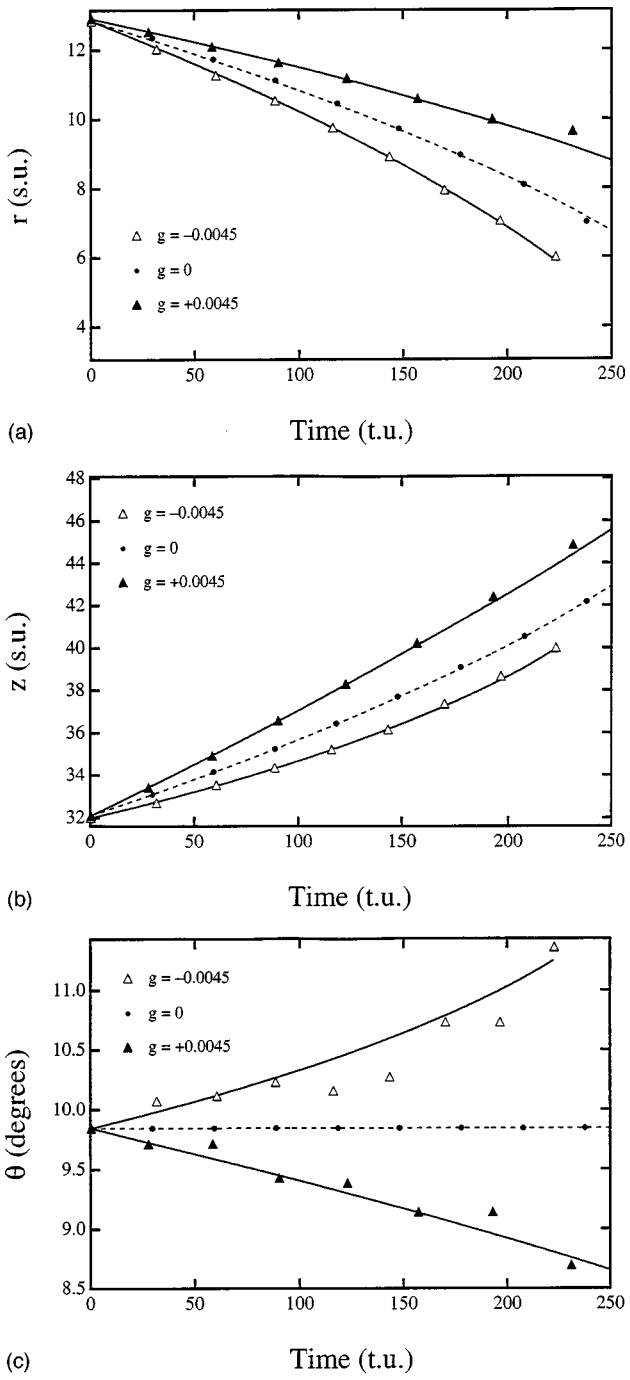

FIG. 4. Comparison of local theory (lines) and simulation (triangles and circles) for initial $\theta = 9.8°$, with three different gradients. r is in space units (s.u.); time is in time units (t.u.). (a) The radius of the ring as a function of time. (b) The vertical (z) position of the center of the ring. (c) The angle θ of the ring with respect to the z axis. The simulations were carried out using the modified FitzHugh-Nagumo equations (see Appendix B for numerical details) on a computational grid of size $80 \times 80 \times 80$, with $h_x = 0.75$ s.u. and $h_t = 0.04$ t.u. The gradient was implemented as a gradient in the parameter c_2, varying from 0.75 to 1.02. The theoretical curves were computed using $\alpha = 0.24$, $\beta = \pm 0.0056$, $\gamma = \pm 0.01$, and $\mu = 0.43$. These values for α and μ were determined from the zero-gradient simulation, and the values for β and γ were estimated from the drift of a two-dimensional spiral in an identical gradient.

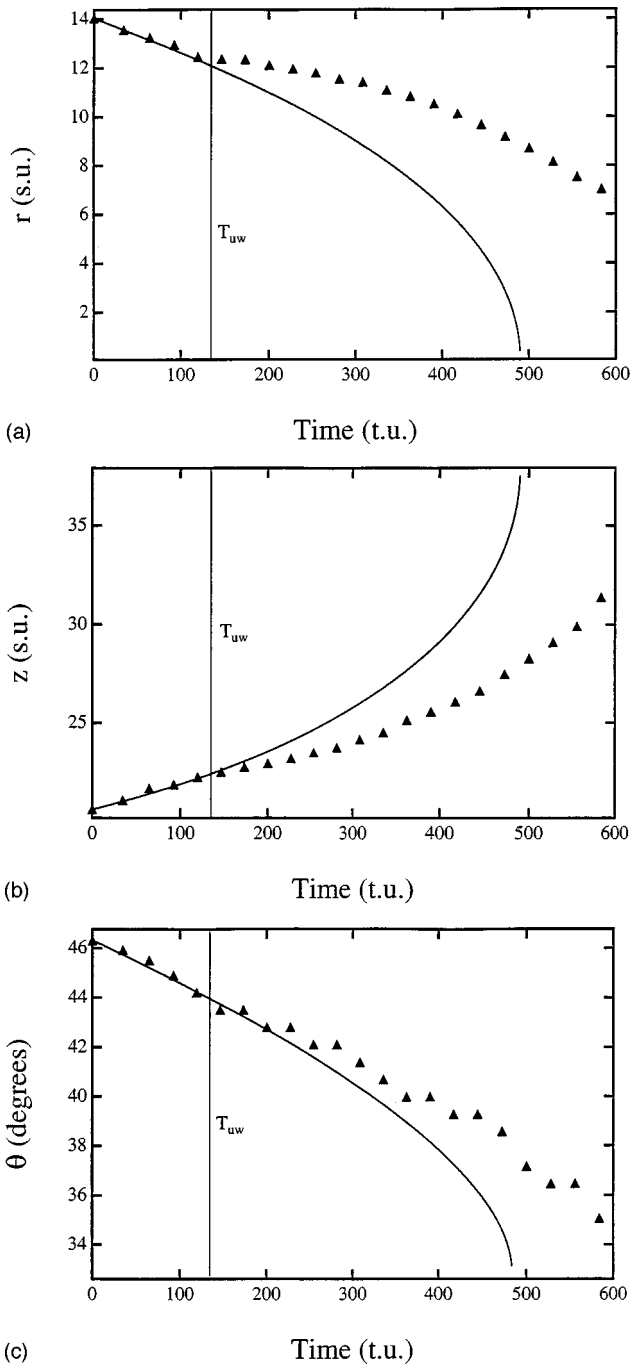

FIG. 5. Comparison of local theory and simulation for initial $\theta = 46°$. The gradient here was 0.0045. All other parameters were the same as Fig. 4. The vertical line shows the approximate unwinding time T_{uw}, after which nonlocal effects render the local theory unreliable.

here, we are able to identify the precise mechanism by which the parameter gradient causes deviation from the local theory. The mechanism is the ''unwinding'' effect, which leads to nonlocal interactions of distant parts of the filament [15]. Figure 6 illustrates this effect by showing the scroll wave in cross section through the center. The gradient is oriented so that the lower part of the ring rotates faster. The upper panels show a rotation just after the moment the gradient is applied ($t = 0$). The lower panels show one rotation cycle of the same ring, after the unwinding has developed

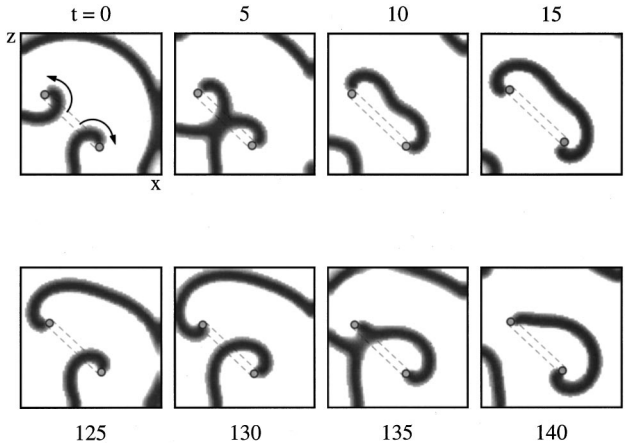

FIG. 6. Cross sections of a scroll ring, showing the unwinding effect. The number for each panel shows the time of the snapshot in t.u. $t=0$ was the moment when the gradient was turned on. The upper row shows the rotation before the unwinding, the lower panel shows the rotation just before T_{uw}. These calculations were done with the same parameters as Fig. 5.

($t=125$ through 140). At $t=0$, the waves are symmetrical, and the wave fronts collide along the ring's axis of symmetry far from the filament (see the panel at $t=5$), and therefore do not affect the motion of the filament. At later times, however, the symmetry is broken: the lower part has accumulated turns of the spiral around it at the expense of the upper part (unwinding), causing the collision point to migrate closer to the upper part of the ring. Now the wave front collides very close to the upper part of the filament itself, directly affecting its motion (the first such collision occurs at the T_{uw}, the unwinding time). This additional filament motion is purely nonlocal, as it is caused by a wave front originating from a distant part of the ring.

The unwinding of the slower (upper) part of the ring filament is due to the differential rotation periods caused by the gradient. The unwinding time may be estimated from the rotation periods at the fastest and slowest parts of the ring via the following equation [29,15]:

$$T_{uw}=\frac{2r}{u(1-\tau_1/\tau_2)}. \tag{6}$$

Here τ_1 is the period of the fastest part of the filament, τ_2 is the period of the slowest part (so that $\tau_1<\tau_2$), r is the radius of the ring, and u is the linear speed of the wave fronts. The periods τ_1 and τ_2 can be obtained by computing the rotation period of two-dimensional spirals at the local parameter values corresponding to the location of the upper and lower parts of the ring. The time T_{uw} calculated from this equation agrees with the observations of the time when the simulations begin to deviate significantly from the theory (see Fig. 5).

If the ring shrinks and disappears before it has a chance to unwind, then the local theory should hold, even for large angles. The applicability of the local theory therefore should depend on the relative size of two time scales: the unwinding time, given by Eq. (6), and the lifetime of the ring, T_{life}, which may be obtained from Eqs. (5). That is, the theory applies whenever

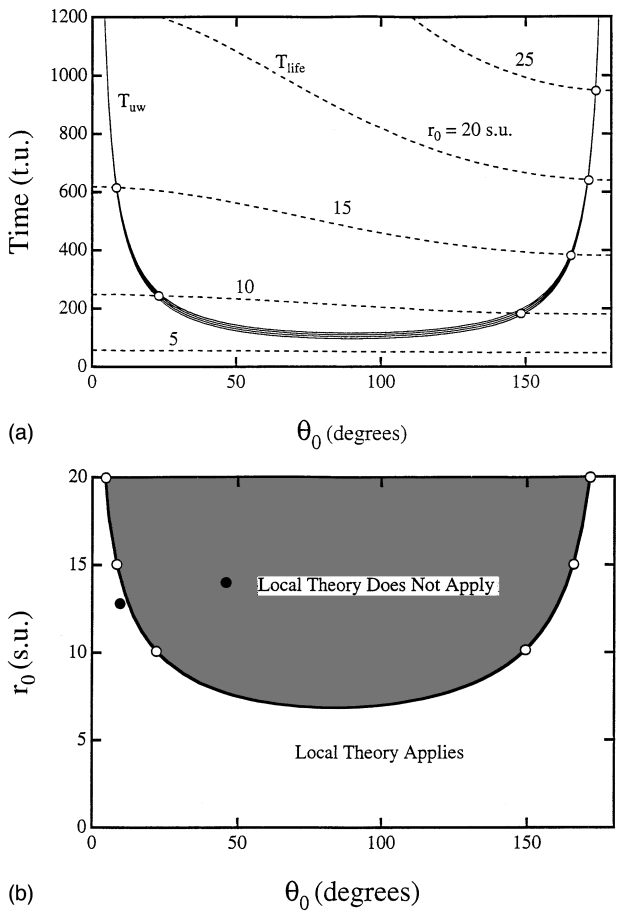

FIG. 7. (a) Unwinding time (solid) and lifetime (dashed), as functions of initial angle, for several different initial radii. These curves were derived using the same parameters as Figs. 4–6. The T_{uw} curves were computed using Eq. (6); the values of τ_1 and τ_2 for each angle were computed using a polynomial fit to the spiral wave period as a function of c_2, as determined from two-dimensional runs. The T_{life} curves were obtained by numerically integrating Eqs. (5) using a fourth-order Runge-Kutta algorithm, until the radius r reached zero. (b) Parameter plane of initial radius and angle, showing the region for which the local theory may be expected to work. The open circles correspond to the open circles in (a), and the dark circles show the initial conditions for Figs. 4 and 5.

$$T_{uw}>T_{life}. \tag{7}$$

The lifetime may be calculated by integrating Eqs. (5) until the radius reaches zero. It should be noted that when the gradient is strong enough that the ring expands, T_{life} is infinite, and a conservative estimate predicts that the theory should fail for nonzero angles.

Figure 7(a) shows T_{uw} (solid lines) and T_{life} (dashed lines) as functions of the initial angle for several different initial radii, using parameters obtained from the FitzHugh-Nagumo simulations of Figs. 4–6. T_{uw} is large for angles close to 0 and 180° (because in such cases the rotation periods τ_1 and τ_2 are nearly equal), and decays rapidly as the angle approaches 90°. The T_{life} curves depend weakly on angle and strongly on initial radius. The intersections of these families of curves give the limits of the applicability of the local theory, leading to Fig. 7(b). As can be seen, for angles close to 0 and 180° the theory applies for a wide range of initial

radius. The two cases shown in Fig. 4 (where the theory applies) and Fig. 5 (where it does not) are indicated in Fig. 7 as filled circles. As expected, the point that falls above the curve in Fig. 7(b) corresponds to a simulation in which the theory did not hold, and the point that falls below it corresponds to a simulation where the theory did hold.

Figure 7(b) was computed for a single value of the gradient. A stronger gradient will decrease the unwinding time, leading to a smaller region of applicability of the local theory. To gauge the strength of the gradient in a model-independent fashion, the nondimensional strength of the gradient, as measured by its effect on the time scales of the system, may be taken to be $\Delta T/T_s$, where ΔT is the difference in spiral wave periods over the diameter of the ring [approximately, $\Delta T=(dT/dz)(2r)$, where dT/dz is the gradient in rotation period, evaluated at the center of the ring], and T_s is the spiral wave period at the center of the ring. For the simulations of Fig. 4, ΔT was approximately 12 time units (t.u.), and T_s was 27 t.u., for a dimensionless value of $\Delta T/T_s=0.44$. This shows that the modified local theory may work even though the (nondimensional) gradient is not very small.

In addition to the nonlocal effects described here, there may be other mechanisms of deviation between the modified local theory and the simulations. For example, due to the differential rotation periods, twist must develop along the ring filament, and this may affect the dynamics (although to lowest order of the local theory, twist does not affect the motion of the filament [20,21]). For larger twist rates, the effect on the filament dynamics can be significant [30,13].

IV. CONCLUSION

In this paper, we propose equations of motion for scroll ring filaments in a parameter gradient. These equations predict reorientation of the plane of the ring, acceleration or deceleration of its collapse (or expansion), and an additional component of its drift, so that it no longer drifts along its axis of symmetry. The equations work well unless nonlocal effects due to self-interaction of widely separated parts of the ring rotating at different rates become important. We give explicit conditions under which this occurs.

Although in this paper we tested the modified local theory using only the FitzHugh-Nagumo model, we expect the results reported here to hold for other models of excitable media as well. Moreover, we believe a similar extension of the local theory to include the effect of the gradient may also work for other scroll wave configurations, with similar limitations imposed by nonlocal effects.

ACKNOWLEDGMENTS

This work was supported in part by National Heart and Blood Institute Grant No. HL39707. M.V. acknowledges support from a Pennsylvania SSHE Professional Development grant. We thank Dr. Omer Berenfeld, Dr. Vadim Biktashev, and Dr. Marcel Wellner for their careful reading of the paper and several valuable suggestions.

APPENDIX A: DERIVATION OF EQS. (5)

For the parametrization given in Eq. (3), the unit tangent vector at point p is [using the fact that $ds/dp=r$ for the circular ring of Eq. (3), where s denotes arclength]

$$\hat{\mathbf{T}}=\frac{d\mathbf{R}/dp}{ds/dp}=-\sin p\,\hat{\mathbf{y}}-(\cos\theta\hat{\mathbf{x}}+\sin\theta\hat{\mathbf{z}})\cos p, \tag{A1}$$

the unit normal vector is (using the fact that $\kappa=1/r$ for the ring)

$$\hat{\mathbf{N}}=\frac{1}{\kappa(ds/dp)^2}\left[\frac{d^2\mathbf{R}}{dp^2}-\frac{d^2s}{dp^2}\hat{\mathbf{T}}\right]=-\cos p\,\hat{\mathbf{y}}+(\cos\theta\hat{\mathbf{x}}+\sin\theta\hat{\mathbf{z}})\sin p, \tag{A2}$$

and the unit binormal vector is

$$\hat{\mathbf{B}}=\hat{\mathbf{T}}\times\hat{\mathbf{N}}=-\sin\theta\hat{\mathbf{x}}+\cos\theta\hat{\mathbf{z}}. \tag{A3}$$

Note that the binormal vector is independent of p; that is, it is the same for all parts of the ring. Using Eq. (2), we find for the two components of the gradient-induced velocity

$$\mathbf{G}_\perp=\beta(g)(-\sin p\hat{\mathbf{x}}+\cos\theta\cos p\hat{\mathbf{y}}),\qquad \mathbf{G}_\parallel=\gamma(g)\hat{\mathbf{z}}. \tag{A4}$$

Using these expressions for $\hat{\mathbf{T}}$, $\hat{\mathbf{N}}$, and the two components of $\mathbf{G}$, Eq. (1) immediately gives us the right-hand side of Eq. (4). We now differentiate Eq. (3) with respect to time, obtaining

$$\frac{d\mathbf{R}_p}{dt}=\dot{x}\hat{\mathbf{x}}+\dot{r}\cos p\,\hat{\mathbf{y}}-\dot{r}(\cos\theta\hat{\mathbf{x}}+\sin\theta\hat{\mathbf{z}})\sin p-r(-\dot{\theta}\sin\theta\hat{\mathbf{x}}+\dot{\theta}\cos\theta\hat{\mathbf{z}})\sin p, \tag{A5}$$

where we use the dots to denote time derivatives. We equate Eq. (A5) to the right-hand side of Eq. (4), equate x, y, and z components, and Eqs. (5) immediately follow.

APPENDIX B: NUMERICAL MODEL

The results of this paper were tested computationally using the modified FitzHugh-Nagumo model [23,24,31,10]:

$$\frac{\partial E}{\partial t}=f(E)-g+D\nabla^2E,\qquad \frac{\partial g}{\partial t}=(E-g)/\tau(E). \tag{B1}$$

Here E is the excitation of the medium; g is the recovery. Time is measured in time units and space in space units (s.u.).

The function $f(E)$ is chosen to be a piecewise linear, ''N''-shaped function:

$$f(E)=\begin{cases}-c_1E & \text{for } E<E_1\\ c_2(E-a) & \text{for } E_1\leqslant E\leqslant E_2\\ -c_3(E-1) & \text{for } E>E_2\end{cases} \tag{B2}$$

and $\tau(E)$ is piecewise constant:

$$\tau(E)=\begin{cases}\tau_1 & \text{for } E<B_1\\ \tau_2 & \text{for } B_1\leqslant E\leqslant B_2\\ \tau_3 & \text{for } E>B_2.\end{cases} \tag{B3}$$

The parameter values for the functions defined above used in this paper are as follows: $c_1=4.0$, $c_3=15.0$, $E_1=0.018$, $\tau_1=\tau_3=0.5$, $\tau_2=16.66$, $B_1=0.01$, $B_2=0.95$. The parameters E_2 and a are determined by demanding continuity of the function $f(E)$: $E_2=[(c_1+c_2)E_1+c_3]/(c_3+c_2)$, $a=E_1(c_1+c_2)/c_2$. The gradient was implemented as a linear variation in the parameter c_2 (generally varying between 0.75 and 1.02).

To solve Eqs. (B1), an explicit Euler scheme was carried out on a regular lattice with space step $h_x=0.75$ s.u. and time step $h_t=0.04$ t.u. These were chosen so that a further decrease produced no significant change in the final results.

The core of the scroll ring was determined by tracking the maximum value of E over one rotation period, and defining the core to consist of those points whose maximum value is below a certain threshold value (generally chosen to be halfway between the maximum and minimum values of E throughout the lattice). This procedure produces a ''cloud'' of core points. The filament was then determined in the following way. The center of mass of the ''cloud'' of core points was computed and taken to be the center of the ring. Then the plane that best fit the cloud was determined by computing the mean-square deviation between the cloud of points and a plane of given angle; the angle θ that gave least mean-square deviation was taken to be the plane of the ring (and the magnitude of the deviation was then a measure of how planar the ring actually was). Once the plane was determined, a cylindrical coordinate system was imposed on it, with the center of mass as the origin: (ρ,ϕ,z). The filament was computed as $\rho(\phi)$ and $z(\phi)$, determined by least-squares fitting Fourier series to those functions.

As for initial conditions, scroll rings were produced by initiating a spherical wave in the center of the medium (by stimulating at a point), and then killing off half the medium, above a plane inclined by angle θ with respect to the z direction, when the sphere reached a specified size. This procedure produced a circular wave break that subsequently became a scroll ring inclined by θ. In all cases, one rotation period was allowed to pass before the gradient was switched on.

APPENDIX C: STABILITY

Here we address the stability of Eqs. (5) as solutions to the full differential geometry equations (1). Equations (5) describe a ring which remains planar and circular. But are the solutions of these equations stable solutions of the full equations of motion Eq. (1)? In particular, if the ring deviates slightly from its planar, circular shape, do the perturbations grow or shrink? To answer these questions, we have compared solutions of Eqs. (5) with numerical solutions of Eq. (1). Figure 8 shows an example in which the filament is given a perturbation that significantly distorts it from its planar, circular shape. As can be seen, the perturbations die out very rapidly, returning the filament to its planar shape. In addition, using the numerical scheme with a smaller perturbation, we find that the filament converges to the solutions of Eqs. (5) (not shown).

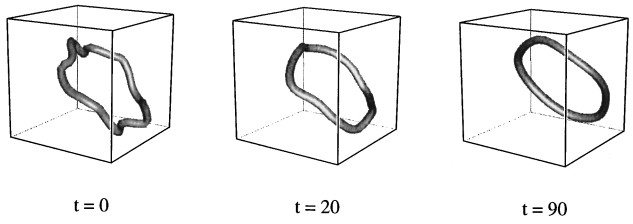

FIG. 8. Filament images, showing stability of the planar, circular ring. These figures were obtained by integrating the full differential geometry equations (1) by discretizing the filament with 256 points and numerically integrating $d\mathbf{R}/dt$. The initial conditions were a ring with both normal and binormal perturbations. At $t=20$, the perturbations have noticeably shrunk, and by $t=90$, the filament has almost returned to its planar, circular shape.

The stability question may also be addressed analytically. For example, consider binormal perturbations to the flat ring, so that $\mathbf{R}(p)$ becomes

$$\mathbf{R}(p)=\mathbf{R}_0(p)+\epsilon\sin np\hat{\mathbf{B}}, \tag{C1}$$

where n is the (integer) frequency of the perturbation, ϵ is its magnitude, $\hat{\mathbf{B}}$ is the binormal unit vector to the (unperturbed) ring, and $\mathbf{R}_0(p)$ is given by Eq. (3). Then inserting this equation into Eq. (1), to linear order in ϵ we find

$$\frac{d\epsilon}{dt}=-\frac{\alpha n^2}{r^2}\epsilon. \tag{C2}$$

Since $\epsilon^{-1}d\epsilon/dt$ is negative for all n, the perturbations decay to zero. (The parameter α is positive for most systems of experimental relevance. When it is negative [21,27], or when the gradient is sufficiently strong, the ring tends to grow and perturbations do not decay.) Although ϵ goes to zero, the ring itself may shrink as well, and for shape stability we actually need ϵ/r to go to zero. Analysis of Eq. (C2) shows that this condition holds for all $n>1$. For the case $n=1$, the binormal perturbation is equivalent to a rotation of the ring, and can be absorbed by a redefinition of θ.

[1] J. M. Davidenko, A. M. Pertsov, R. Salomonsz, W. Baxter, and J. Jalife, Nature (London) **335**, 349 (1992).
[2] A. T. Winfree, Science **266**, 1003 (1994).
[3] F. Siegert and C. Weijer, Physica D **49**, 224 (1991).
[4] A. M. Zhabotinsky and A. N. Zaikin, *Oscillatory Processes in Biological and Chemical Systems* (Nauka, Pushchino, Russia, 1971), Vol. 2.
[5] A. T. Winfree, Science **175**, 634 (1972).
[6] G. S. Skinner and H. L. Swinney, Physica D **48**, 1 (1991).

[7] R. R. Aliev and A. B. Rovinsky, J. Phys. Chem. **96**, 732 (1992).
[8] V. G. Fast and A. M. Pertsov, J. Cardiovasc. Electrophysiol. **3**, 255 (1992).
[9] O. Steinbock, J. Schütze, and S. C. Müller, Phys. Rev. Lett. **68**, 248 (1992).
[10] A. M. Pertsov and M. Vinson, Philos. Trans. R. Soc. London, Ser. A **347**, 687 (1994).
[11] A. M. Zhabotinsky, S. C. Müller, and B. Hess, Physica D **49**, 47 (1991).
[12] M. Vinson, A. M. Pertsov, and J. Jalife, Physica D **72**, 119 (1993).
[13] S. Mironov, M. Vinson, S. Mulvey, and A. Pertsov, J. Phys. Chem. **100**, 1975 (1996).
[14] M. Vinson, S. Mironov, S. Mulvey, and A. M. Pertsov, Nature (London) **386**, 477 (1997).
[15] M. Vinson, Physica D **116**, 313 (1998).
[16] A. V. Panfilov and A. M. Pertsov, Dokl. Biophys. **274**, 58 (1984).
[17] W. Jahnke, C. Henze, and A. Winfree, Nature (London) **336**, 662 (1988).
[18] A. V. Panfilov, A. N. Rudenko, and V. I. Krinsky, Biofizika **31**, 850 (1986).
[19] J. P. Keener, Physica D **31**, 269 (1988).
[20] J. P. Keener and J. J. Tyson, SIAM (Soc. Ind. Appl. Math.) Rev. **34**, 1 (1992).
[21] V. N. Biktashev, A. V. Holden, and H. Zhang, Philos. Trans. R. Soc. London, Ser. A **347**, 611 (1994).
[22] A. M. Pertsov and Ye. A. Yermakova, Biofizika **33**, 338 (1988) [Biophysics **33**, 364 (1998)].
[23] R. FitzHugh, Biophys. J. **1**, 445 (1961).
[24] A. M. Pertsov, E. A. Ermakova, and A. V. Panfilov, Physica D **14**, 117 (1984).
[25] A. B. Rovinsky and A. M. Zhabotinsky, J. Phys. Chem. **88**, 6081 (1984).
[26] A. B. Rovinsky, J. Phys. Chem. **90**, 217 (1986).
[27] V. N. Biktashev, Int. J. Bifurcation Chaos Appl. Sci. Eng. **8**, 677 (1998).
[28] A. T. Winfree, in *Chemical Waves and Patterns*, edited by R. Kapral and K. Showalter (Kluwer, Dordrecht, 1995), pp. 3–55.
[29] V. I. Krinsky and K. I. Agladze, Physica D **8**, 50 (1983).
[30] C. Henze, E. Lugosi, and A. T. Winfree, Can. J. Phys. **68**, 683 (1990).
[31] E. A. Ermakova, A. M. Pertsov, and E. E. Shnol, Physica D **40**, 185 (1989).